Shootin1 Regulates Retinal Ganglion Cell Neurite Development: Insights From an RGC Direct Somatic Cell Reprogramming Model

Ke Zhang,[1] Tingting Zhang,[1] Qinghai He,[1] Huilin Liang,[1] Jingyi Guo,[1] Mingbing Zeng,[1,2] and Shuyi Chen[1]

[1]State Key Laboratory of Ophthalmology, Zhongshan Ophthalmic Center, Sun Yat-Sen University, Guangdong Provincial Key Laboratory of Ophthalmology and Visual Science, Guangzhou, China
[2]Hainan Eye Hospital and Key Laboratory of Ophthalmology, Zhongshan Ophthalmic Center, Sun Yat-Sen University, Haikou, China

Correspondence: Shuyi Chen, State Key Laboratory of Ophthalmology, Zhongshan Ophthalmic Center, Sun Yat-Sen University, Guangdong Provincial Key Laboratory of Ophthalmology and Visual Science, 7 Jinsui Road, Tianhe District, Guangzhou 510623, China; chenshy23@mail.sysu.edu.cn. Mingbing Zeng, Hainan Eye Hospital and Key Laboratory of Ophthalmology, Zhongshan Ophthalmic Center, Sun Yat-Sen University, 19 Xiuhua Road, Xiuying District, Haikou 570311, China; zengmigb@mail.sysu.edu.cn.

Received: February 1, 2024
Accepted: June 10, 2024
Published: June 27, 2024

Citation: Zhang K, Zhang T, He Q, et al. Shootin1 regulates retinal ganglion cell neurite development: Insights from an RGC direct somatic cell reprogramming model. *Invest Ophthalmol Vis Sci.* 2024;65(6):41. https://doi.org/10.1167/iovs.65.6.41

Purpose. Retinal ganglion cells (RGCs) connect the retina to the brain. Proper development of the axons and dendrites of RGCs is the basis for these cells to function as projection neurons to deliver visual information to the brain. The purpose of this study was to investigate the function of *Shtn1* (which encodes shootin1) in RGC neurite development.

Methods. Immunofluorescence (IF) was used to characterize the expression pattern of marker genes. An in vitro direct somatic cell reprogramming system was used to generate RGC-like neurons (iRGCs), which was subsequently used to study the function of *Shtn1*. Short-hairpin RNAs (shRNAs) were used to knock down *Shtn1*, and the coding sequence (CDS) of *Shtn1* was used to overexpress the gene. Lentiviruses were used to deliver shRNAs or CDSs into iRGCs. The patch clamp technique was used to measure the electrophysiological properties of the iRGCs. RNA sequencing (RNA-seq) was used to examine transcriptome expression.

Results. Using IF, we demonstrated that shootin1 is distinctively expressed in RGCs during the period in which RGCs actively develop and adjust the connections of their neurites with upstream and downstream neurons. Using the iRGC system, we demonstrated that *Shtn1* promotes the growth and complexity of neurites and thus the electrophysiological maturation, of iRGCs. RNA-seq analyses showed that *Shtn1* may also regulate gene expression and neurogenesis in iRGCs.

Conclusions. *Shtn1* promotes RGC neurite development. These findings improve our understanding of the molecular machinery governing RGC neurite development and may help to optimize future RGC regeneration methods.

Keywords: *Shtn1*, retinal ganglion cells, axon growth, dendrite development, induced neuron

Retinal ganglion cells (RGCs) are the sole projection neurons in the retina that are responsible for delivering the electrophysiological signals generated by visual circuits in the retina to the visual center in the brain to form vision and other light-related physiological functions.[1–3] RGCs are also among the most vulnerable neurons in the retina and are often damaged in prevalent retinal degeneration diseases, such as glaucoma and optic nerve neuropathy, leading to irreversible blindness.[4,5] To function as projection neurons in the retina, RGCs must form complex but highly organized dendritic connections with bipolar and amacrine interneurons in the retina. These connections are the structural basis of the delicate and diverse vision-related electrophysiological properties of RGCs. RGCs also must project axons long distances to the visual center and form proper topographic projection maps with central neurons in this region. These circuits are the structural basis for the precise processing of visual information and various visual-based physiological processes.[6–8] During development, upon becoming postmitotic, RGCs migrate to the ganglion cell layer and begin the long process of structural and functional refinement. RGC axons are generated soon after the birth of RGCs, whereas RGC dendrites develop later when other late-born retinal interneurons, such as amacrine cells and bipolar cells, are generated.[9] After their initial establishment, both the axons and dendrites of RGCs undergo active sprouting and pruning to interpret environmental guidance cues to establish visual circuit networks with upstream interneurons within the retina or downstream neurons in the visual center of the brain.[9–11] Although promoting the regeneration of RGCs in situ or delivering exogeneous RGCs through transplantation are promising strategies for treating RGC-related blinding diseases, reestablishing neurite connections between regenerated RGCs and

their upstream and downstream neurons is one of the major hurdles preventing the application of these regenerative medicine strategies.[12–15] Thus, how RGC neurite development is controlled is an important biological question and is a subject under active investigation in the field.

We previously characterized the unique transcriptome of the optic fissure, which is the pathway through which the growing axons of newly generated RGCs exit the developing retina.[16] Among the genes that are specifically expressed in the optic fissure region are those that are involved in regulating neurite development, indicating roles for these genes in regulating RGC axon guidance. *Shtn1* (which encodes the protein shootin1) is one such gene. Studies using cultured hippocampal neurons have shown that shootin1 is a key molecule that regulates neuronal polarity and neurite growth by modulating the coupling of filamentous actin (F-actin) dynamics with cell adhesion molecules in response to neuronal activities and extracellular cues.[17–20] During our subsequent examination of the shootin1 protein expression pattern in the retina, we observed that, in addition to being expressed in the closing optic fissure, shootin1 exhibited a distinct expression pattern in RGCs during the active axon and dendrite remodeling period, indicating a role of shootin1 in RGC neurite development. Exploiting an in vitro RGC direct somatic cell reprogramming system we recently established,[21] we demonstrated that *Shtn1* is an important regulator of neurite development in RGCs. These findings improve our understanding of the molecular machinery governing RGC axon and dendrite development and may help to optimize future RGC regeneration methods.

Methods

Cell Culture and Virus Packaging

All animal studies were performed in adherence with the ARVO Statement for the Use of Animals in Ophthalmic and Vision Research and were approved by the Zhongshan Ophthalmic Center Animal Care and Use Committee. Mouse embryo fibroblasts (MEFs) were isolated from E13.5 mouse embryos as previously described. Briefly, embryos were collected in cold PBS. The head, spinal cord, and all internal organs were removed, and the remaining tissue was cut into small pieces. The tissue was digested using TrypLE Express Enzyme (Thermo Fisher Scientific, Waltham, MA, USA) at 37°C for 15 minutes to create a single-cell suspension. The cells were plated on a 15-cm dish in MEF medium supplemented with Dulbecco's modified Eagle's medium (DMEM; Thermo Fisher Scientific), 10% fetal bovine serum (FBS; Biowest, Nuaillé, France), MEM nonessential amino acids (NEAAs; Thermo Fisher Scientific), and penicillin/streptomycin (Thermo Fisher Scientific). The cells were passaged once before being frozen in liquid nitrogen for future use. To prepare lentiviruses, HEK293 cells were transfected with gene expression lentivirus plasmids, together with the two packaging plasmids, psPAX2 and pMD2.G (Addgene, Watertown, MA, USA). Thirty-six hours after transfection, the viral supernatants were collected, concentrated, and frozen for future use.

RGC-Like Neuron Reprogramming

RGC-like neuron (iRGC) reprogramming was performed as previously described with minor modifications. Briefly, frozen MEFs were thawed and cultured in MEF medium on plates precoated with poly-D-lysine and laminin following the published instructions.[22] On the second day after plating, The MEFs were infected with the pSicoR-TetON-ABI lentivirus. After 16 to 20 hours, the cells were switched to fresh MEF medium containing doxycycline (2 µg/mL; Sigma-Aldrich, St. Louis, MO, USA). After 48 hours, the medium was switched to neuronal culture medium (DMEM/Nutrient Mixture F-12 containing GlutaMAX, penicillin/streptomycin, N2, and B27; all from Thermo Fisher Scientific) and forskolin (5 µM; Sigma-Aldrich). Half of the medium was changed every other day.

Molecular Cloning

Short-hairpin RNAs (shRNAs) targeting *Shtn1* were cloned into the pSicoR lentivirus vector (Addgene, Watertown, MA, USA). The targeting shRNA sequences were (1) CCACGGTGAATAAATAGAAAT, and (2) GCGACAAAGCTAAATAAAGAA. The coding sequences (CDSs) of *Shtn1* were PCR-amplified from mouse brain cDNA pools and cloned into the home-modified pSicoR-TetON-3xFLAG vector using the restriction enzyme digestion–ligation method. shRNA#2-refractory *Shtn1* CDSs were constructed by using the following primer pair: GCcACcAAaCTgAAcAAgGAgAATAAAACACTGAAAAGAATC and cTCcTTgTTcAGtTTgGTgGCCAAGGCTTCAGCGCTCTCTC (letters in lower cases indicate mutated nucleotide sequences). Sanger sequencing was used to validate the constructs.

Reprogramming Efficiency Calculation

Forty-eight hours after doxycycline treatment, the cells in one well from each experimental group were fixed and stained for ASCL1. Images were taken with a 10× objective, 10 randomly selected 10× image fields were counted, the number of $ASCL1^+$ transduced cells/field was averaged, and the total number of $ASCL1^+$ transduced cells/well was calculated based on the area of the field under the 10× objective relative to that of the entire well. At different time points during iRGC reprogramming, the cells were fixed and stained for TUJ1. $TUJ1^+$ cells with thin cellular processes three times longer than the cell body were judged as iRGCs. The total number of iRGCs/well was calculated in the same way as for $ASCL1^+$ transduced cells/well 48 hours after doxycycline induction, as described above. Finally, the reprogramming efficiency was calculated by dividing the number of iRGCs/well with the number of $ASCL1^+$ cells/well 48 hours after doxycycline induction. At least three biological replicate experiments were performed, and the numbers were averaged and are presented with standard deviations.

Neurite Length Measurement

On the fifth day of iRGC reprogramming, the cells were washed with PBS, fixed with 4% paraformaldehyde (PFA; Sigma-Aldrich) in PBS for 10 minutes at room temperature, and immunostained with anti-TUJ1 antibodies for the neurite length assay. The neurite length was measured and quantified using ImageJ (National Institutes of Health, Bethesda, MD, USA). For $TUJ1^+$ cells, the neurite length was measured by quantifying the distance from the center of the cell body to the tip of the longest process. For iRGCs at day 13 after induction of ABI expression (DAI 13), MEFs were co-infected with low-titer mCherry-expressing lentiviruses to sparsely

label the iRGCs, and the neurite lengths of the sparsely labeled iRGCs were measured as described above.

Immunofluorescence Staining

To obtain tissue cryosections, the embryos and eyes of wild-type C57BL/6J mice were fixed overnight at 4°C in 4% PFA, dehydrated with 15% and 30% sucrose (Sigma-Aldrich), frozen in Tissue-Tek O.C.T. freezing medium (Sakura Finetek, Tokyo, Japan), and sectioned using a cryomicrotome (CM1950; Leica, Wetzlar, Germany). For cultured cells, cells were fixed with 4% PFA for 10 minutes at room temperature and washed with PBS containing 0.1% Triton X-100 (PBST; Sigma-Aldrich). The samples were blocked with 5% normal serum (Jackson ImmunoResearch, West Grove, PA, USA) in PBST for at least 30 minutes, incubated with primary antibody for 2 hours at room temperature or 4°C overnight, washed with PBST, incubated with secondary antibody for 1 hour at room temperature, washed with PBST three times, incubated with 4′,6-diamidino-2-phenylindole (DAPI, 1 µg/mL; Sigma-Aldrich) to stain the nuclei for 5 minutes at room temperature, and washed with PBST three times. The stained cells were observed and imaged under a Zeiss Axio Observer Z7 inverted microscope or a Zeiss LSM 980 confocal microscope. The antibodies used were mouse anti-TUJ1 (G7121, 1:1000; Promega, Madison, WI, USA), rabbit anti-TUJ1 (802001, 1:1000; BioLegend, San Diego, CA, USA), rabbit anti-ASCL1 (ab74065, 1:500; Abcam, Cambridge, MA, USA), rabbit anti-SHTN1(PA5-11091, 1:200; Abcam), mouse anti-FLAG(F1804, 1:1000; Sigma-Aldrich), and Alexa Fluor 488-, 568-, or 647-conjugated secondary antibodies (1:1000; Thermo Fisher Scientific).

Electrophysiology

Cells were grown on gelatin-coated coverslips (VWR, Radnor, PA, USA). The coverslips were placed in a recording chamber (0.5 mL in volume) on the fixed stage of an upright microscope (BX51WI; Olympus, Tokyo, Japan) equipped with epifluorescence optics and a 40× water-immersion objective lens. The cells were continuously perfused with oxygenated bicarbonate-buffered artificial cerebrospinal fluid (ACSF; 119-mM NaCl, 26.2-mM $NaHCO_3$, 11-mM glucose, 2.5-mM KCl, 1.0-mM K_2HPO_4, 2.5-mM $CaCl_2$, and 1.3-mM $MgCl_2$). Step current injection–evoked action potentials were recorded in current-clamp mode, with current steps at 10-pA intervals. Whole-cell currents were recorded in voltage-clamp mode with a basal holding potential of −70 mV and voltage steps ranging from –70 to +30 mV at 10-mV increments. Stimulus delivery and data acquisition were carried out via an EPC 10 amplifier (HEKA, Frankfurt, Germany). The data were digitized at 10 kHz with a 3-kHz lowpass filter and analyzed with Patchmaster (HEKA). The liquid junction potential was corrected to 13.3 mV.

RNA Sequencing

Infected cells were collected 5 days after doxycycline induction by FACS using a BD FACSAria Fusion Flow Cytometer (BD Biosciences, San Jose, CA, USA). For each RNA sequencing (RNA-seq) experiment, 1×10^6 cells were used. Three biological replicates were performed for each group of cells. Sequencing libraries were generated using the NEBNext Ultra RNA Library Prep Kit for Illumina (New England Biolabs, Ipswich, MA, USA). The libraries were sequenced on an Illumina HiSeq platform (Illumina, San Diego, CA, USA), and 150-bp paired-end reads were generated.

RNA-Seq Data Analyses

The raw reads were filtered and trimmed to remove the adapters using Trimmomatic to obtain clean reads. The clean reads were aligned to the mouse reference genome (mm10) using HISAT2. FeatureCounts was used to count the reads mapped to each gene. Differential gene expression analysis was performed using the DESeq2 R package (R Foundation for Statistical Computing, Vienna, Austria). Genes with an adjusted $P < 0.05$ and fold change >2 were considered differentially expressed genes. Gene Ontology (GO) term enrichment analysis and Gene Set Enrichment Analysis (GSEA) were performed using clusterProfiler.

Statistical Analysis

All experiments whose data were subjected to statistical analysis were performed with at least three biological replicates. Quantitative data are presented as the mean ± SD or mean ± SEM. *P* values were evaluated by either Student's *t*-test or one-way ANOVA test.

Data Availability

Sequencing data have been deposited in the Gene Expression Omnibus (GEO) under accession code GSE254839.

Results

Shootin1 Is Distinctively Expressed in Developing RGCs Undergoing Active Neurite Growth and Remodeling

Using transcriptome comparison and mRNA in situ hybridization, we previously demonstrated that *Shtn1* mRNA is specifically expressed in the closing optic fissure area.[16] To further characterize the expression pattern of *Shtn1* during retinal development, we performed immunofluorescent (IF) staining using an anti-shootin1 antibody. IF staining of embryonic day 11.5 (E11.5) mouse retinal sagittal sections showed that the shootin1 protein was specifically expressed in retinal progenitor cells surrounding the closing optic fissure (Fig. 1A), consistent with the *Shtn1* mRNA expression pattern we reported previously.[16] By further observing shootin1 expression in later stages of the developing retina, we interestingly found that shootin1 exhibited a distinct, yet dynamic, expression pattern in RGCs. Except for those around the closing optic fissure region, undifferentiated retinal progenitor cells did not express shootin1 (Fig. 1A). Around E12.5, accompanying the appearance of the first-born RGCs, shootin1 expression was highly and specifically upregulated in newborn RGCs (Fig. 1B, where the arrows point to $TUJ1^+$ newborn RGCs). Such high and specific expression of shootin1 in RGCs continued through the postnatal period, when the dendritic and axonal connections of RGCs with other retinal neurons and visual center neurons were actively being modified and refined (Fig. 1C, where the RGCs are labeled by BRN3A and the arrow points to a displaced RGC in the neuroblastic layer). In addition to the high level of shootin1 expression in the soma of RGCs, shootin1 expression was also observed in the developing inner plexiform layer (IPL) and the nerve fiber layer,

Investigative Ophthalmology & Visual Science

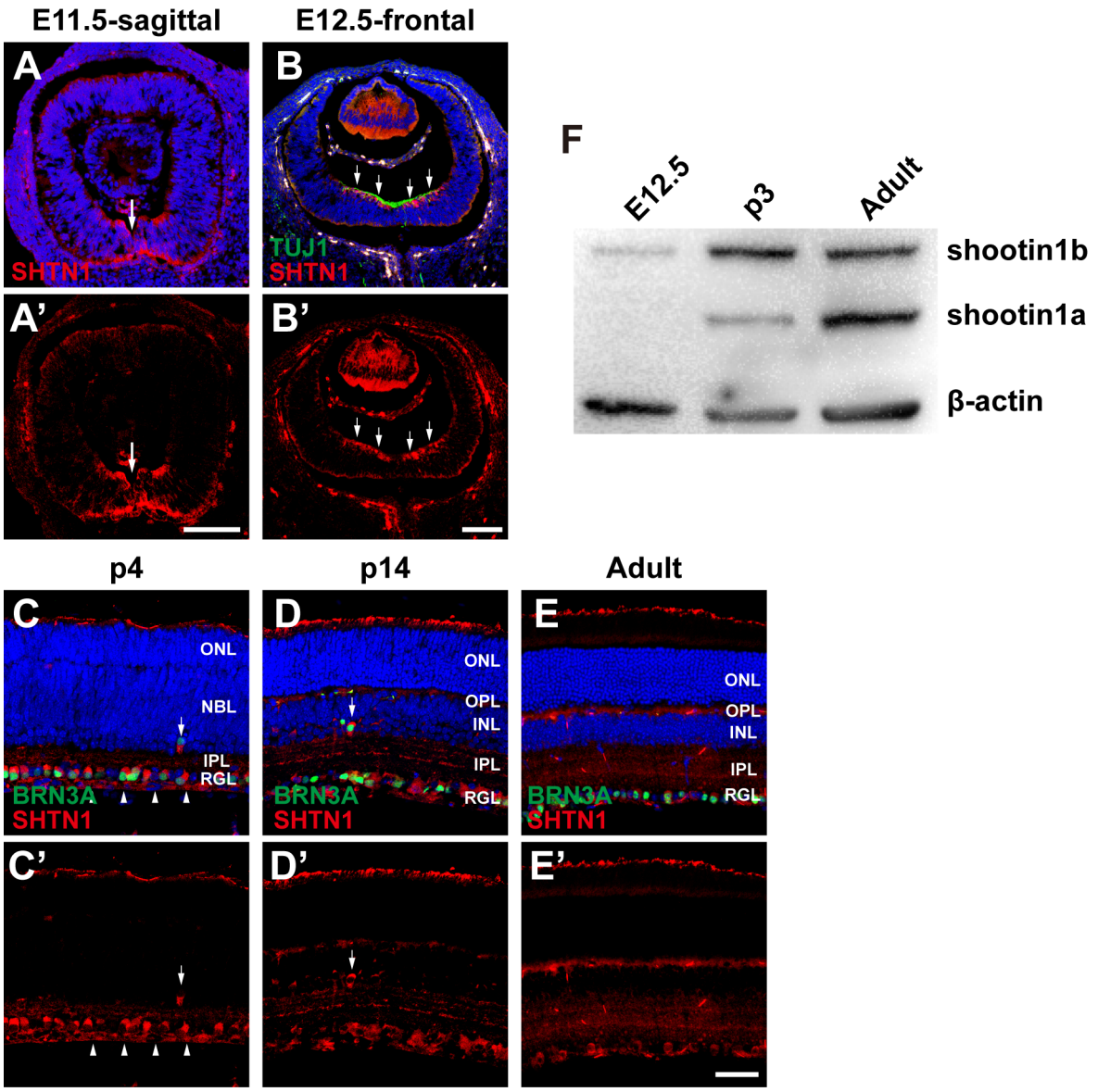

Figure 1. Shootin1 is distinctively expressed in developing RGCs in vivo. (**A–E**) Confocal images of the retinas of mice of different ages stained for shootin1 (*red*) and RGC markers (*green*). The *arrow* in **A** points to the closing optic fissure. The *arrows* in **B** point to TUJ1^{+} (*green*) newborn RGCs. The *arrowheads* in **C** point to the nerve fiber layer where the axons of RGCs project. The *arrows* in **C** and **D** point to RGCs (labeled by BRN3A) displaced in the neuroblastic layer (**C**) or inner nuclear layer (**D**). Shootin1 expression patterns (*red*) are highlighted by showing individual channels in the bottom panels. *Scale bars:* 100 µm (**A'**, **B'**) and 50 µm (**E'**). (**F**) Western blot analyses of the expression patterns of shootin1a and shootin1b in the retinas of different developmental stages. INL, inner nuclear layer; IPL, inner plexiform layer; NBL, neuroblastic layer; ONL, outer nuclear layer; OPL, outer plexiform layer; RGL, retinal ganglion cell layer.

which harbor the dendrites and axons of RGCs, respectively (Fig. 1C, where the arrowheads point to the nerve fiber layer). The expression of shootin1 in RGCs decreased somewhat from approximately 2 weeks after birth, when retinas gradually reach maturity, but was still maintained in adult mice (Figs. 1D', 1E'). There are two splicing isoforms of shootin1: shootin1a and shootin1b. Shootin1a is the shorter form of shootin1 that is 456 amino acids (aa) long, whereas in shootin1b the last 3 aa of shootin1a are substituted by 178 aa residues[23] (Fig. 1F). To examine which isoform of shootin1 is expressed in the retina, we performed western blot analyses on tissue lyses of retinas of different developmental ages. The results showed that, at E12.5, when RGCs begin to be generated in the retina, weak shootin1b was detected in the retina, but there was no shootin1a expression at the time. At postnatal day 3 (p3) when RGC generation has finished and RGCs are actively adjusting their axonal and dendritic connections with other neurons, the expression level of shootin1b increased, and shootin1a was also expressed in the retina, although the expression level of shootin1a was lower than that of shootin1b. In adult retinas, both shootin1a and shootin1b continued to be expressed in the retina, but the expression of shootin1a increased to a level even stronger than that of shootin1b (Fig. 1F). Thus, shootin1 exhibited a distinct expression pattern in developing RGCs, in the period when the dendritic and axonal connections of these cells with upstream and downstream neurons were being actively modified and refined,

Investigative Ophthalmology & Visual Science

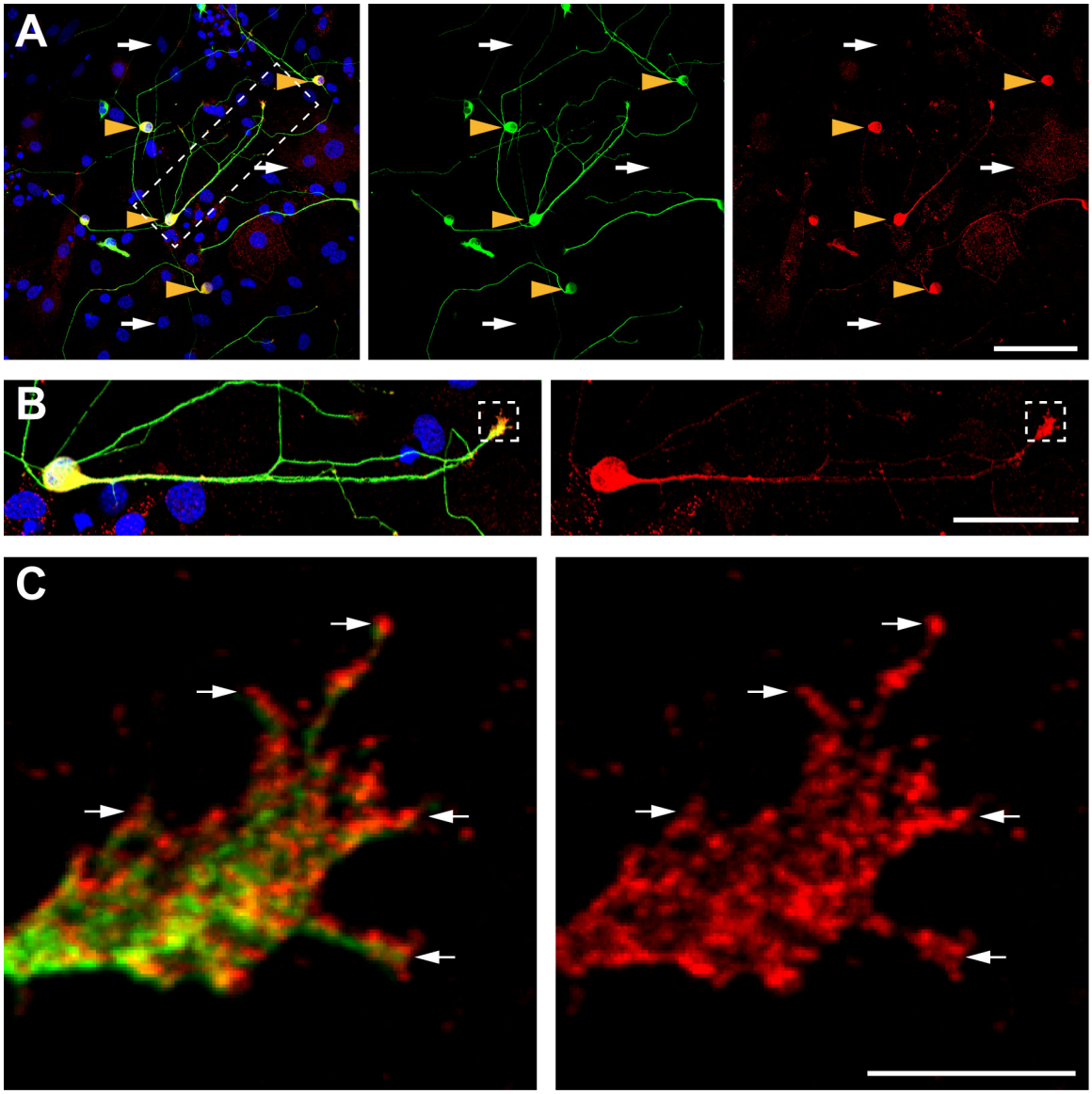

Figure 2. Shootin1 is specifically expressed in reprogrammed iRGCs in vitro. Confocal images of iRGCs stained for shootin1 (*red*), TUJ1 (*green*, indicating successfully reprogrammed iRGCs), and nuclei (DAPI, *blue*). The area outlined by the *dashed line* in **A** is shown at a higher magnification in **B**, and the growth cone area outlined by the *dashed line* in **B** is shown at a higher magnification in **C**. The *white arrows* in **A** point to MEFs that were not infected with ABI lentivirus. The *yellow arrowheads* in **A** point to TUJ1$^+$ successfully reprogrammed iRGCs. The *arrows* in **C** point to the tip of the filipodia where shootin1 accumulated. *Scale bars:* 100 µm (**A**), 50 µm (**B**), and 5 µm (**C**).

suggesting that *Shtn1* may play a role in RGC neurite development.

Shootin1 Accumulates at the Growth Cones of RGCs Induced In Vitro

In vitro cultured neurons are excellent models for studying the molecular and cellular mechanisms governing neurite development. We thus sought to establish an in vitro culture system to study the function of *Shtn1* in RGCs. Native RGCs can be isolated from dissociated retinal tissues through immunopanning.[24] However, this process is tedious, and the number of RGCs obtained is limited. We recently developed a direct somatic cell reprogramming method that can efficiently generate RGC-like neurons in vitro, in which by overexpressing three transcription factors, *Ascl1*, *Brn3b*, and *Islet1* (ABI), MEFs can be efficiently reprogrammed to become iRGCs within 13 days. These neurons resemble RGCs at the transcriptome level and electrophysiological functional levels and thus represent an excellent in vitro model for studying RGC biology.[21] To evaluate this system to study the function of *Shtn1*, we first examined the expression of shootin1 in iRGCs. MEFs did not express it or expressed it at only a low level (Fig. 2A, where the white arrows point to MEFs that were not infected with ABI-overexpressing lentivirus). However, when MEFs were reprogrammed into TUJ1$^+$ iRGCs, shootin1 expression was dramatically upregulated (Fig. 2A, yellow arrowheads). The shootin1 protein was distributed both in the soma and along the neurites of the iRGCs (Fig. 2B). The nerve growth cone is the migrating tip of growing neurites and plays a central

Investigative Ophthalmology & Visual Science

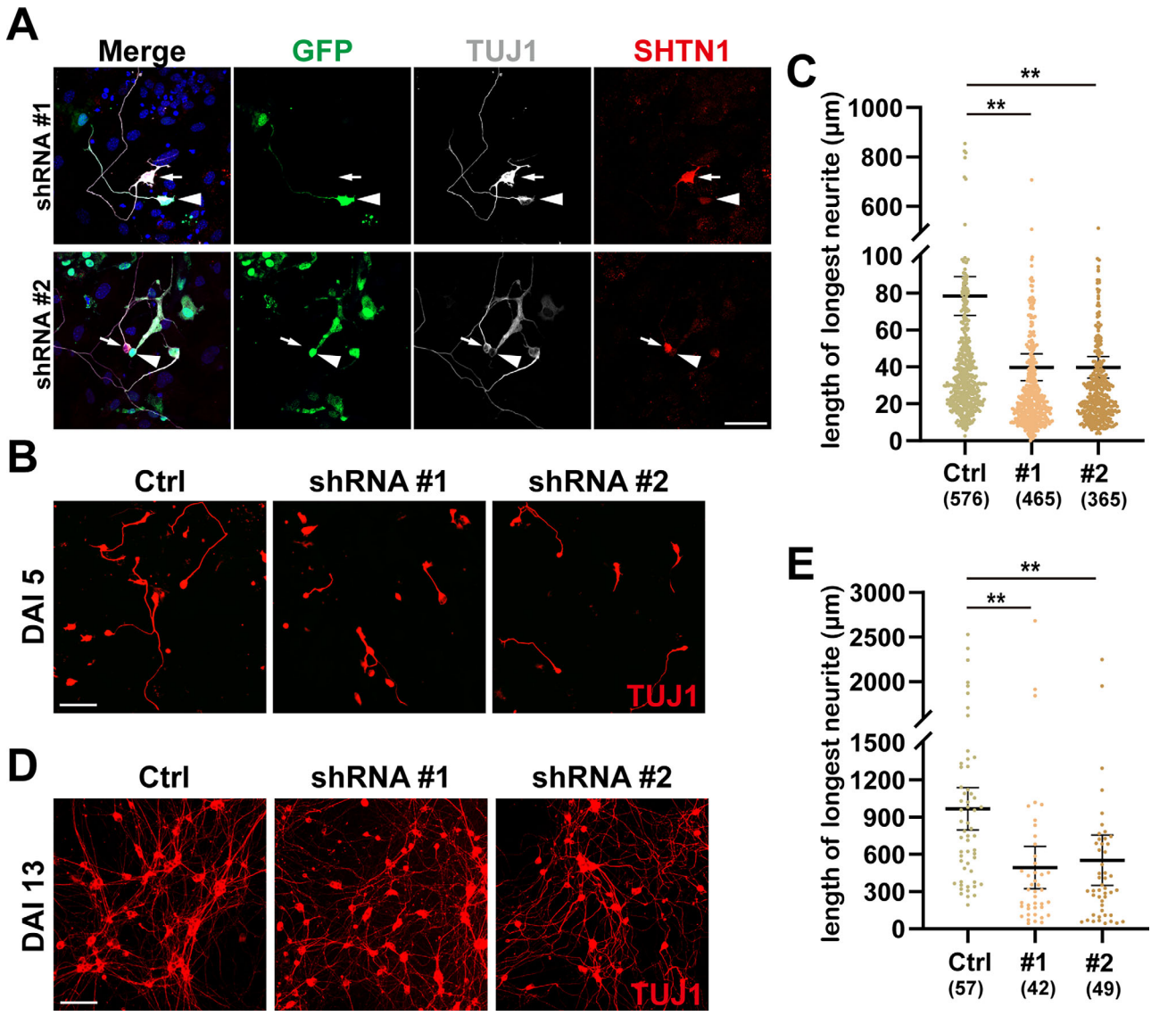

Figure 3. *Shtn1* deficiency retards the growth of iRGC axons. (**A**) IF images showing that shRNAs targeting *Shtn1* abolished the expression of shootin1 in iRGCs. The *arrows* point to iRGCs that were not infected with shRNA-expressing lentivirus (indicated by lack of GFP expression), and the *arrowheads* point to iRGCs expressing shRNAs (indicated by GFP expression). (**B**) IF images of TUJ1-stained iRGCs from the control and *Shtn1*-knockdown groups at DAI 5. (**C**) A plot showing the measurement results of the length of iRGC axons in **B**. Numbers inside the *brackets* indicate the number of iRGCs measured. (**D**) IF images of TUJ1-stained iRGCs from the control and *Shtn1*-knockdown groups at DAI 13. (**E**) A plot showing the measurement results of the length of iRGC axons in **D**. Numbers inside the *brackets* indicate the number of iRGCs measured. $^{**}P < 0.01$ (one-way ANOVA was used to compare each shRNA group with the control group). *Scale bars*: 50 μm (**A**) and 100 μm (**B**, **D**).

role in neurite outgrowth. Intriguingly, shootin1 abundantly accumulated at the growth cones of growing iRGC neurites (Fig. 2B, dashed boxes), especially at the edge of the extending filopodia of the growth cone (Fig. 2C, white arrows). The significant upregulation of shootin1 in reprogrammed iRGCs and its distinct polarized accumulation pattern in the growth cones of developing neurites suggest that *Shtn1* may play important roles in regulating iRGC neurite development.

Shtn1 Deficiency Retards the Growth of iRGC Axons

To investigate the role of *Shtn1* in iRGC neurite development, we designed two shRNAs against *Shtn1* and coinfected MEFs with *Shtn1*–shRNA-expressing lentiviruses and ABI-overexpressing lentiviruses. IF staining of shootin1 on day 13 of reprogramming culture showed that shootin1 was abundantly expressed in successfully reprogrammed iRGCs as shown above (Fig. 3A, arrows). Both *Shtn1*-targeting shRNAs dramatically reduced the expression level of shootin1, demonstrating that the two shRNAs efficiently knocked down *Shtn1* (Fig. 3A, where the arrowheads point to green fluorescent protein [GFP]$^{+}$ shRNA-expressing cells). To examine the effects of *Shtn1* knockdown on iRGC neurite development, we slightly modified our iRGC reprogramming system by performing the experiments on poly-D-lysin/laminin–coated plates to make the system more suitable for investigating shootin1-mediated neurite extension effect.[22,25] We chose to examine iRGCs on day 5 after induc-

tion of ABI expression (DAI 5), which is the time point at which the newly converted iRGCs were in the early stages of neurite development. At DAI 5, many iRGCs contained one long neurite, representing an axon (Fig. 3B, Ctrl). We measured the length of the iRGCs axons. The length of the iRGC axons at DAI 5 mostly ranged from 23.00 to 79.03 µm (25%–75%), with a mean ± SEM length of 78.25 ± 5.347 µm in the control group (n = 576 cells; three experiments) (Figs. 3B, 3C). Interestingly, knocking down *Shtn1* by either shRNA significantly reduced the length of the iRGC axons: The length of the iRGC axons in the shRNA #1 group mostly ranged from 13.00 to 39.32 µm (25%–75%), with a mean length of 39.78 ± 3.688 µm (P < 0.0001, one-way ANOVA; n = 465 cells; three experiments), whereas the length of the iRGC axons in the shRNA #2 group ranged from 15.04 to 38.47 µm (25%–75%), with a mean length of 39.70 ± 2.956 µm (P < 0.0001, one-way ANOVA; n = 365 cells; three experiments) (Figs. 3B, 3C), demonstrating that *Shtn1* knockdown prohibited the growth of the axons of iRGCs. At DAI 13, neurites of iRGCs in both the control and *Shtn1*-shRNA knockdown groups had extended long distances. Measurements of the neurite length showed that neurites in the shRNA groups were still shorter than those in the control group (control: mean ± SEM, 966.8 ± 85.59 µm; shRNA#1: 492.2 ± 84.69 µm, P = 0.0011; shRNA#2: 552.3 ± 100.9 µm, P = 0.0033, one-way ANOVA) (Figs. 3D, 3E). Thus, these results demonstrated that *Shtn1* deficiency retarded the growth of iRGC axons.

Shtn1 Overexpression Promotes the Complexity of iRGC Neurites

To further investigate the role of *Shtn1* in iRGC neurite development, we examined the effects of overexpressing *Shtn1* in iRGCs. We constructed lentiviruses expressing shootin1a and shootin1b and cotransfected MEFs with ABI-overexpressing lentiviruses and FLAG-tagged *Shtn1*-overexpressing lentiviruses. We examined iRGCs at DAI 5 to measure the length of the axons. Surprisingly, similar to what was observed following *Shtn1* knockdown, overexpressing either *Shtn1a* or *Shtn1b* also reduced the length of iRGC axons (Figs. 4A, 4B). The axon length of iRGCs overexpressing *Shtn1a* ranged mostly from 16.08 to 46.14 µm (25%–75%), with a mean ± SEM length of 47.68 ± 3.741 µm (n = 383 cells; three experiments), and that of iRGCs overexpressing *Shtn1b* ranged mostly from 14.03 to 62.17 µm (25%–75%), with a mean length of 63.33 ± 6.297 µm (n = 310 cells; three experiments); the axons of both of these groups were significantly shorter than those of the iRGCs in the control group (P < 0.0001 and P = 0.0022 for *Shtn1a*- and *Shtn1b*-overexpression groups, respectively; one-way ANOVA), which ranged mostly from 24.16 to 86.38 µm (25%–75%), with a mean length of 87.81 ± 5.385 µm (n = 636 cells; three experiments) (Fig. 4B). Thus, overexpressing *Shtn1* also impeded the extension of iRGC axons.

However, unlike those in the *Shtn1* knockdown groups, we noticed that iRGCs overexpressing either *Shtn1a* or *Shtn1b* tended to have multiple neurite branches extending from the cell body (Figs. 4A, 4C). We thus quantified the number of neurite branches that extended from the soma of iRGCs at DAI 5. In the control group, more than half of the iRGCs had no established neurite structures; whereas, for those that exhibited neurite structures, most of them had only one long neurite, some had two neurites, and only a small portion of them had more than two neurites (Figs. 4A, 4D; the asterisks in Fig. 4A indicate iRGCs with one neurite). However, more iRGCs in the *Shtn1a/b*-overexpressing groups than in the control group had obvious neurite structures (Figs. 4A, 4D). Quantification of the number of neurite branches showed that, in the control group, 17.81% ± 4.65% iRGCs (mean ± SD) had more than two neurites, whereas much larger proportions of iRGCs in the shootin1a-overexpressing group (26.05% ± 10.58%; P = 0.0291, Student's t-test) and shootin1b-overexpressing group (30.45% ± 4.62%; P = 0.0002, Student's t-test; six experiments) had more than two neurites (Figs. 4A, 4D; the white arrows in Fig. 4A, Shtn1a/1b, point to iRGCs with multiple neurites). More intriguingly, many *Shtn1a/b*-overexpressing iRGCs extended numerous cellular processes from their cell bodies, which were obviously in the active growth phase, as indicated by the enlarged growth cone structures enriched for FLAGed-shootin1 at the tips of the processes (Fig. 4C, highlighted by red arrows). Moreover, many DAI 13 iRGCs overexpressing either *Shtn1a* or *Shtn1b* exhibited sophisticated structures at the distal end of neurites (Fig. 4E, where representative iRGCs overexpressing *Shtn1a/b* are highlighted in the enlarged images). These results demonstrate that *Shtn1* promotes the establishment of neurites in iRGCs and thus may increase the complexity of the neurite networks iRGCs can form. We also measured the length of neurites of iRGCs overexpressing *Shtn1* at DAI 13. The results showed that the neurites in the *Shtn1a*-overexpression group were still shorter (mean ± SEM, 391.4 ± 55.59 µm; n = 47; P < 0.0001, one-way ANOVA) than those in the control group (966.8 ± 85.59 µm; n = 57), whereas those in the *Shtn1b*-overexpressing group were similar (923.7 ± 108.7 µm; n = 52; P = 0.7237) to those in the control group (Fig. 4F).

Disruption of *Shtn1* Compromises the Electrophysiological Properties of iRGCs

To determine whether *Shtn1* deficiency affects the electrophysiological maturation of iRGCs, we performed patch-clamp recording of iRGCs at DAI 7 and DAI 13. The depolarizing resting membrane potential of the iRGCs in the *Shtn1*-knockdown groups was similar to that of the control iRGCs at both DAI 7 and DAI 13 (Fig. 5A). However, iRGCs deficient in *Shtn1* displayed slightly compromised K^+ currents, especially at DAI 7 (Fig. 5B), and iRGCs of the shRNA #2 group displayed significantly decreased Na^+ currents at both DAI 7 (P = 0.0084, Student's t-test; seven cells in each group) and DAI 13 (P = 0.00049, Student's t-test; seven cells in each group) (Fig. 5C). To test whether the decreased Na^+ current phenotype was caused by shRNA off-targeting, we constructed shRNA #2–refractory *Shtn1a*- and *Shtn1b*-overexpressing plasmids, and coexpressed these plasmids with shRNA #2. The results showed that overexpressing either *Shtn1a* or *Shtn1b* could rescue the decreased Na^+ current phenotype (Supplementary Fig. S1), suggesting that the phenotype was caused by *Shtn1* knockdown.

Consistent with the compromised K^+ and Na^+ currents, iRGCs deficient in *Shtn1* displayed a compromised ability to fire action potentials, which was more severe for the shRNA #2 group (Figs. 5D, 5E). At DAI 7, all iRGCs (n = 7) in the control group examined were able to fire action potentials, and over half of them even fired multiple action potentials. In contrast, five out of seven iRGCs in the shRNA #1 group

Investigative Ophthalmology & Visual Science

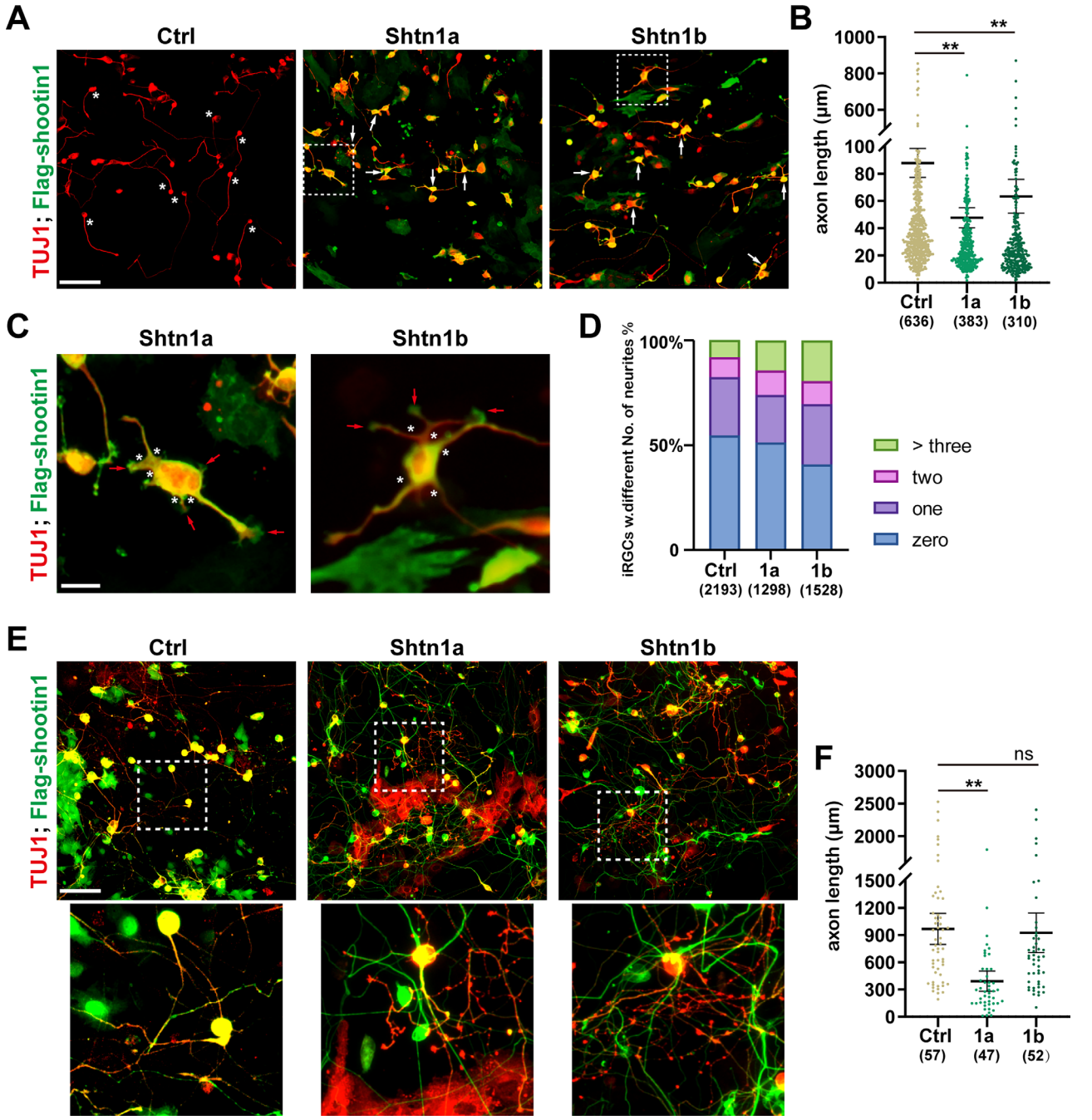

Figure 4. *Shtn1* overexpression increases the complexity of neurites in iRGCs. (**A**) IF images of iRGCs stained for TUJ1 (*red*) and FLAG (*green*, indicating shootin1 expression) in the control and *Shtn1*-overexpressing groups at DAI 5. The areas outlined by the *dashed lines* are shown at higher magnification in **C**. (**B**) A plot showing the length of DAI 5 iRGC axons in the different experimental groups. $^{**}P < 0.01$ (one-way ANOVA). Numbers inside the *brackets* indicate the number of iRGCs measured. (**C**) iRGCs overexpressing either isoform of *Shtn1* exhibit multiple cellular processes extending from their cell bodies. The *asterisks* indicate the root of each cellular process, and the *red arrows* point to the growth cone at the tip of the neurites. (**D**) A plot showing the proportion of iRGCs with different numbers of neurite branches in different experimental groups. Numbers inside the *brackets* indicate the number of iRGCs measured. (**E**) IF images of iRGCs stained for TUJ1 (*red*) and FLAG (*green*, indicating shootin1 expression) in the control and *Shtn1*-overexpressing groups at DAI 13. The areas outlined by the *dashed lines* are shown at a higher magnification in the enlarged images below. (**F**) A plot showing the length of DAI 13 iRGC axons in the different experimental groups. $^{**}P < 0.01$ (one-way ANOVA). Numbers inside the *brackets* indicate the number of iRGCs measured. *Scale bars*: 100 μm (**A**, **E**) and 20 μm (**C**).

fired action potentials, and only two out of seven iRGCs in the shRNA #2 group were able to fire action potentials (Fig. 5E). At DAI 13, most iRGCs in the control and shRNA #1 group fired multiple action potentials; however, iRGCs in the shRNA #2 group could only fire a single action potential, and some failed to exhibit any response (Fig. 5E). Thus, patch clamp recording demonstrated that *Shtn1* deficiency compromised the electrophysiological maturation of iRGCs.

Investigative Ophthalmology & Visual Science

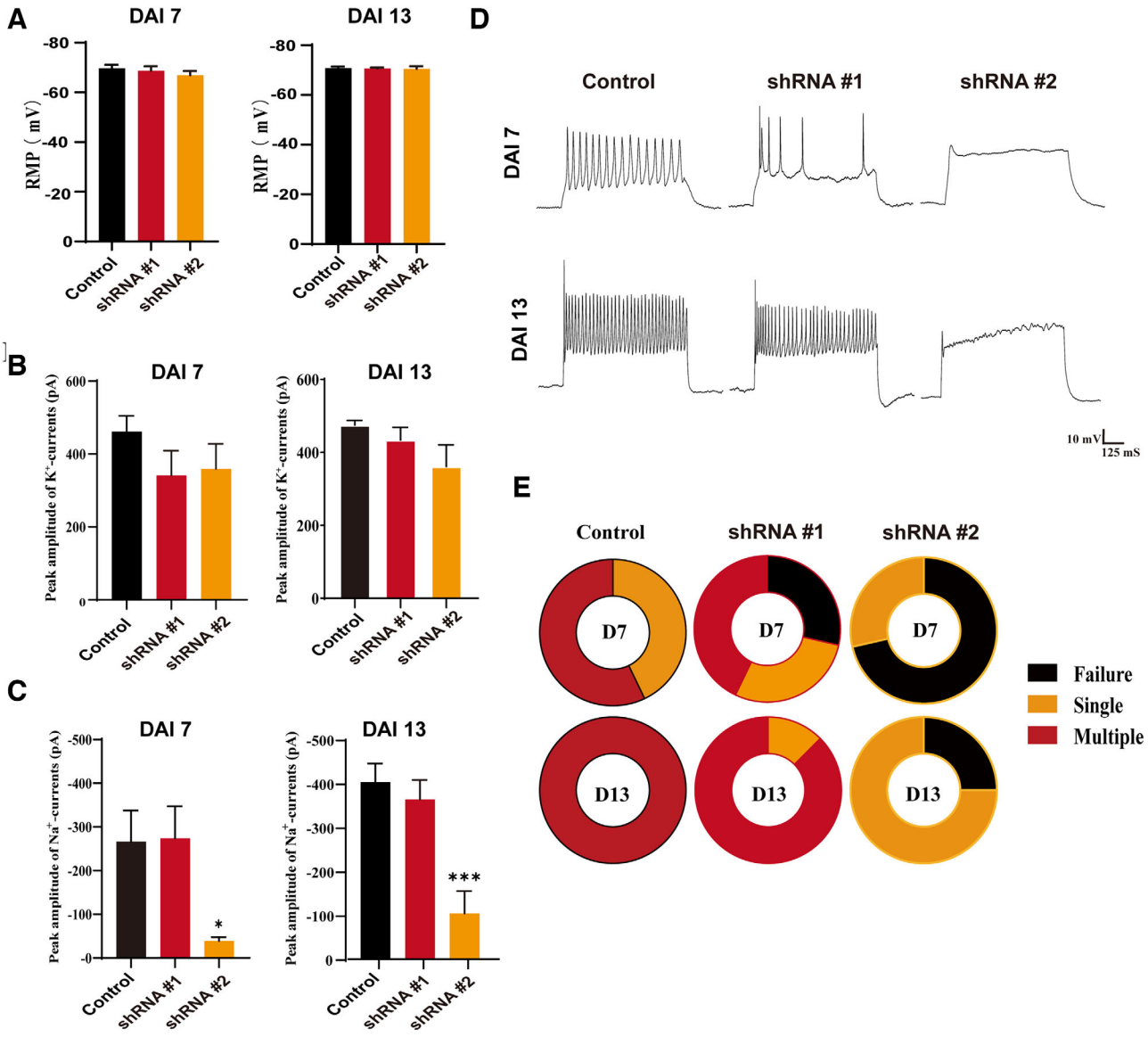

Figure 5. *Shtn1* deficiency compromises the electrophysiological properties of iRGCs. (**A**) Average resting membrane potential (RMP) of iRGCs at DAI 7 and DAI 13; $n = 7$ for each group at DAI 7 and $n = 8$ for each group at DAI 13. The data are represented as mean ± SEM. (**B**) Quantification of the peak amplitudes of K^+ currents in iRGCs from the shRNA and control groups at DAI 7 and DAI 13; $n = 7$ for each group at DAI 7 and $n = 8$ for each group at DAI 13. The data are represented as mean ± SEM. (**C**) Quantification of the peak amplitudes of Na^+ currents in iRGCs from the shRNA and control groups at DAI 7 and DAI 13. $^{**}P < 0.01$ (Student's *t*-test); $n = 7$ for each group at DAI 7 and $n = 8$ for each group at DAI 13. The data are represented as mean ± SEM. (**D**) Representative traces of action potentials recorded in current-clamp mode for iRGCs from the shRNA and control groups at DAI 7 and DAI 13. (**E**) Pie charts showing the fractions of iRGCs in each group capable of generating multiple action potentials (*red*), single action potentials (*orange*), or no action potentials (*black*); $n = 7$ for each group at DAI 7 and $n = 8$ for each group at DAI 13.

Shtn1 Deficiency Compromised iRGC Reprogramming

We next wanted to determine whether *Shtn1* deficiency affects iRGC reprogramming outcomes. We first quantified the efficiency of ABI-induced iRGC reprogramming in the presence or absence of *Shtn1*-shRNAs by calculating the percentage of the number of $TUJ1^+$ neurons at DAI 13 versus the number MEFs expressing ABI at DAI 2. *Shtn1* knockdown reduced the ABI-induced iRGC reprogramming efficiency: In the control group, 21.69% ± 3.57% of the MEFs overexpressing ABI were converted to $TUJ1^+$ iRGCs, whereas 14.69% ± 5.9% and 9.86% ± 2.32% of the MEF overexpressing ABI and deficient for *Shtn1* (GFP^+ cells) were converted to $TUJ1^+$ iRGCs in the *Shtn1*-shRNA #1 and *Shtn1*-shRNA #2 groups, respectively (Figs. 6A, 6C). The reduced iRGC reprogramming efficiency observed at DAI 13 may have been due to a reduced initial induction efficiency or defects in maintaining iRGCs. We thus quantified the $TUJ1^+$ cell induction efficiency at DAI 5. Although the percentage was slightly lower than that in the control group, more than 20% of the MEFs overexpressing ABI were converted to $TUJ1^+$ putative iRGCs in both the *Shtn1*-shRNA #1 and #2 groups (Figs. 6A, 6B). These results suggest that the reduced

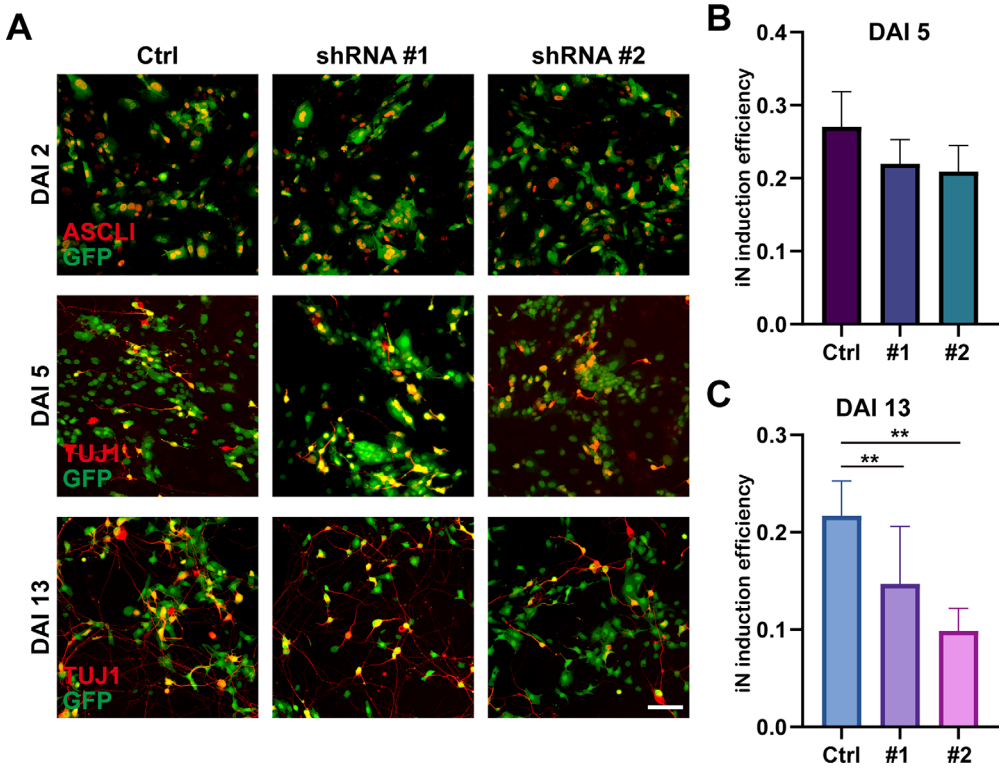

Figure 6. *Shtn1* is required for the iRGC reprogramming process. (**A**) *Upper panels*: IF images of MEFs stained for ASCLI (*red*) and GFP (*green*, indicating control empty vector or shRNA-expressing lentivirus infection) at DAI 2 to show the virus infection efficiency. *Middle panels*: IF images of reprogramming cells stained for TUJ1 (*red*) and GFP (*green*) at DAI 5. *Lower panels*: IF images of reprogramming cells stained for TUJ1 (*red*) and GFP (*green*) at DAI 13. *Scale bar*: 100 µm. (**B**) A plot showing the TUJ1$^+$ iRGC induction efficiency in the control and *Shtn1*-knockdown groups at DAI 5. (**C**) A plot showing the TUJ1$^+$ iRGC induction efficiency in the control and *Shtn1*-knockdown groups at DAI 13. The data are presented as means ± SD, corresponding to three independent biological replicates. $^{**}P < 0.01$ (three biological replicates, Student's *t*-test).

reprogramming efficiency observed at DAI 13 was likely due to defects in the maintenance of the induced iRGCs deficient in *Shtn1*.

Shtn1 Regulates the Expression of Genes Involved in Neurite Development and Neural Fate Induction

Finally, we examined whether *Shtn1* deficiency affects gene expression during iRGC reprogramming. To this end, we isolated reprogramming cells infected with ABI-overexpressing lentiviruses alone or in combination with *Shtn1*-shRNA (#1 and #2)–expressing lentiviruses on DAI 5 and performed RNA-seq. Comparison of the transcriptomes of the *Shtn1*-shRNA group and control group showed that *Shtn1* knockdown caused changes in the expression of only a small group of genes, with most of the differentially expressed genes being downregulated. At the threshold of $P_{adj} < 0.05$ and fold change >2, 445 genes were downregulated, but no genes were upregulated (Fig. 7A). GO enrichment analyses revealed that the genes whose expression was downregulated upon *Shtn1* knockdown were mostly related to neurite and synapse development (Figs. 7B, 7C). The downregulated genes were also enriched for "regulation of neurogenesis" pathways, including many important neurogenic regulators, such as *Lhx1*, *Myt1*, *Myt1l*, *Elavl3*, *Elavl4*, and *Onecut2* (Figs. 7B, 7C). We further performed biological term enrichment analyses to all the sequenced genes by GSEA. Consistent with the results of the GO enrichment analyses, GSEA showed that the activities of the biological processes related to neurite development and neural retina development were suppressed in the *Shtn1* knockdown reprogramming cells (Fig. 7D). Taken together, the transcriptome comparison analyses demonstrated that *Shtn1* knockdown downregulates genes that are important for neural neurite development and neurogenesis.

Discussion

In this study, we discovered that *Shtn1* is distinctively expressed in developing RGCs during the period in which the axonal and dendritic connections of RGCs with upstream and downstream neurons are actively remodeled. Exploiting an in vitro RGC reprogramming system we established recently, we further demonstrated that *Shtn1* plays important roles in regulating the growth and complexity of neurites in RGCs. These findings enrich our understanding of the molecular mechanisms governing RGC axon and dendrite development and may help optimize regenerative therapy protocols for treating RGC-related blinding retinal diseases.

Shootin1 was previously discovered to be a brain-specific protein that regulates axon growth, dendritic spine remodeling, and neuron migration in the brain.[17,18,26,27] However,

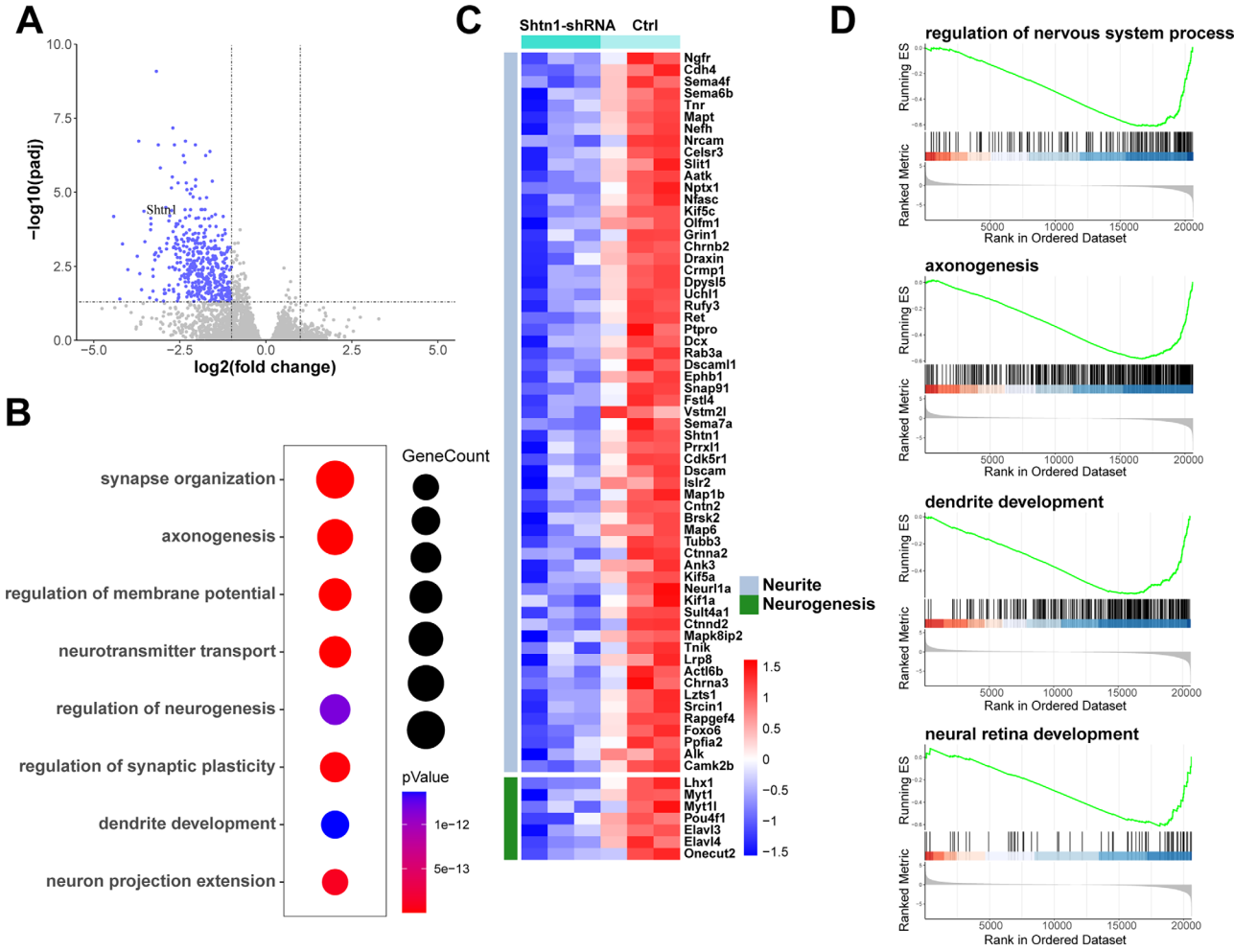

Figure 7. *Shtn1* knockdown caused downregulation of genes related to neurite development and neurogenesis in iRGCs. (**A**) A volcano plot showing gene expression changes upon *Shtn1* knockdown. (**B**) A bubble plot showing the biological pathways enriched in the group of genes downregulated in iRGCs deficient for *Shtn1*. (**C**) A heatmap illustrating that the expression of genes related to neurite development and neurogenesis is downregulated in iRGCs deficient for *Shtn1*. (**D**) GSEA plots illustrating that the biological processes related to neurite development and retinal development are repressed in iRGCs deficient for *Shtn1*.

its expression pattern and role in the retina are unknown. By careful immunohistology examination, we found that the expression pattern of shootin1 in RGCs coincides with the active neurite development periods of the cells. Before differentiation, retinal progenitor cells do not express shootin1; however, upon differentiation, shootin1 is quickly and specifically upregulated in newly generated RGCs. More interestingly, shootin1 expression in RGCs exhibits dynamic changes coinciding with key RGC axon and dendrite remodeling events essential for the establishment of visual circuits, suggesting that shootin1 may play important roles in these processes. Consistent with its specific expression pattern in RGCs in vivo, we found that shootin1 also exhibited a highly specific expression pattern in an in vitro model of RGCs, iRGCs.[21] Careful examination of these in vitro reprogrammed iRGCs revealed that shootin1 was highly and specifically upregulated when MEFs were reprogrammed to an iRGC fate. Within iRGCs, shootin1 abundantly accumulated at the tips of the growth cones of growing axons, the subcellular structures responsible for the growth of the neurites. This distinct expression pattern of shootin1 in iRGCs indicates that the protein plays a role in iRGC neurite development and ensures that iRGCs can be used as a model system for studying the function of *Shtn1* in RGCs.

Exploiting the convenient and quick in vitro iRGC reprogramming system, we studied the role of *Shtn1* in neurite development in iRGCs. Consistent with its highly distinct expression in the growth cones of growing iRGC axons, knocking down *Shtn1* significantly reduced the length of iRGC axons, demonstrating that *Shtn1* promotes the growth of axons of iRGCs. However, paradoxically, overexpressing *Shtn1* also reduced the length of iRGC axons. We believe that these seemingly paradoxical effects of *Shtn1* knockdown and overexpression on axon length reflect two aspects of the function of *Shtn1* in neurite development. On the one hand, during the neurite growth phase, shootin1 functions as a key molecule linking F-actin retrograde flow with the extracellular matrix (ECM) to generate forces to drive the growth of neurites.[18,19,28] Thus, *Shtn1* knockdown disrupts the linkage between F-actin and ECM and reduces the length of iRGC axons. On the other hand, at the beginning of the establishment phase of neurite development, shootin1 functions as a polarity molecule, and its accumulation in certain regions of naïve neurons determines

whether minor cellular processes in those regions eventually lead to neurite outgrowth.[17] Thus, when shootin1 is overexpressed, additional neurites are established in naïve neurons, and because the materials essential for neurite development are limited to one particular neuron, the average length of each neurite is shorter than that of neurons that have only one or two neurites. This is probably what occurs in iRGCs overexpressing *Shtn1*, in which multiple neurites are more common but each neurite is relatively shorter. Thus, the phenotypes observed in *Shtn1* knockdown iRGCs and *Shtn1*-overexpressing iRGCs are consistent with the ability of *Shtn1* to promote the development of iRGC neurites. These neurite development-promoting functions are the cellular basis for the establishment or refinement of visual circuits involving RGCs during development and are also essential for neural circuit network reestablishment after RGC regeneration or transplantation in glaucoma patients; thus, these functions have important biological and translational implications.

Shtn1 knockdown also reduced the ABI-induced iRGC reprogramming efficiency, as measured at DAI 13. However, at DAI 5, a comparable percentage of ABI-overexpressing MEFs were converted to TUJ1$^+$ putative iRGCs. Thus, *Shtn1* is required for the maintenance of induced neurons. It is possible that defective neurite development in *Shtn1*-deficient iRGCs decreases the fitness of reprogramming cells and increases their chance of death. On the other hand, RNA-seq analyses of reprogramming cells at DAI 5 showed that several important neurogenic genes were downregulated in *Shtn1*-deficient reprogramming cells. In addition to its cytoskeleton regulatory function, *Shtn1* can also regulate neural stem cell differentiation by regulating signal transduction.[29] Thus, *Shtn1* may also directly regulate the iRGC reprogramming process by regulating gene expression. RNA-seq analyses showed that many genes essential for neurite development were significantly downregulated in *Shtn1*-deficient reprogramming cells. Thus, *Shtn1* may also regulate iRGC neurite development by regulating gene expression. In the future, the direct interaction of shootin1 with its partner molecules should be characterized to reveal the downstream mechanisms by which SHTN1 is involved in neurite development and RGC fate determination.

Acknowledgments

The authors thank the staff of the Laboratory Animal Center at the State Key Laboratory of Ophthalmology, Zhongshan Ophthalmic Center, for technical support.

Supported by grants from Guangzhou Municipal Science and Technology (2023A03J0190), National Natural Science Foundation of China (82060176, 81870659), Natural Science Foundation of Hainan Province (822MS190), and Hainan Province Clinical Medical Center.

Disclosure: **K. Zhang**, None; **T. Zhang**, None; **Q. He**, None; **H. Liang**, None; **J. Guo**, None; **M. Zeng**, None; **S. Chen**, None

References

1. Xiang M, Zhou H, Nathans J. Molecular biology of retinal ganglion cells. *Proc Natl Acad Sci USA*. 1996;93:596–601.
2. Hoon M, Okawa H, Della Santina L, Wong RO. Functional architecture of the retina: development and disease. *Prog Retin Eye Res*. 2014;42:44–84.
3. Masland RH. The fundamental plan of the retina. *Nat Neurosci*. 2001;4:877–886.
4. Jonas JB, Aung T, Bourne RR, Bron AM, Ritch R, Panda-Jonas S. Glaucoma. *Lancet*. 2017;390:2183–2193.
5. Jenkins TM, Toosy AT. Optic neuritis: the eye as a window to the brain. *Curr Opin Neurol*. 2017;30:61–66.
6. Sanes JR, Masland RH. The types of retinal ganglion cells: current status and implications for neuronal classification. *Annu Rev Neurosci*. 2015;38:221–246.
7. Coombs JL, Van Der List D, Chalupa LM. Morphological properties of mouse retinal ganglion cells during postnatal development. *J Comp Neurol*. 2007;503:803–814.
8. Dhande OS, Huberman AD. Retinal ganglion cell maps in the brain: implications for visual processing. *Curr Opin Neurobiol*. 2014;24:133–142.
9. Sernagor E, Eglen SJ, Wong RO. Development of retinal ganglion cell structure and function. *Prog Retin Eye Res*. 2001;20:139–174.
10. Tian N. Developmental mechanisms that regulate retinal ganglion cell dendritic morphology. *Dev Neurobiol*. 2011;71:1297–1309.
11. Erskine L, Herrera E. The retinal ganglion cell axon's journey: insights into molecular mechanisms of axon guidance. *Dev Biol*. 2007;308:1–14.
12. Miltner AM, La Torre A. Retinal ganglion cell replacement: current status and challenges ahead. *Dev Dyn*. 2019;248:118–128.
13. Calkins DJ, Pekny M, Cooper ML, Benowitz L, Lasker/IRRF Initiative on Astrocytes and Glaucomatous Neurodegeneration Participants. The challenge of regenerative therapies for the optic nerve in glaucoma. *Exp Eye Res*. 2017;157:28–33.
14. Stern JH, Tian Y, Funderburgh J, et al. Regenerating eye tissues to preserve and restore vision. *Cell Stem Cell*. 2018;22:834–849.
15. Williams PR, Benowitz LI, Goldberg JL, He Z. Axon regeneration in the mammalian optic nerve. *Annu Rev Vis Sci*. 2020;6:195–213.
16. Cao M, Ouyang J, Liang H, et al. Regional gene expression profile comparison reveals the unique transcriptome of the optic fissure. *Invest Ophthalmol Vis Sci*. 2018;59:5773–5784.
17. Toriyama M, Shimada T, Kim KB, et al. Shootin1: a protein involved in the organization of an asymmetric signal for neuronal polarization. *J Cell Biol*. 2006;175:147–157.
18. Shimada T, Toriyama M, Uemura K, et al. Shootin1 interacts with actin retrograde flow and L1-CAM to promote axon outgrowth. *J Cell Biol*. 2008;181:817–829.
19. Toriyama M, Kozawa S, Sakumura Y, Inagaki N. Conversion of a signal into forces for axon outgrowth through Pak1-mediated shootin1 phosphorylation. *Curr Biol*. 2013;23:529–534.
20. Baba K, Yoshida W, Toriyama M, et al. Gradient-reading and mechano-effector machinery for netrin-1-induced axon guidance. *eLife*. 2018;7:e34593.
21. Wang J, He Q, Zhang K, et al. Quick commitment and efficient reprogramming route of direct induction of retinal ganglion cell-like neurons. *Stem Cell Reports*. 2020;15:1095–1110.
22. Minegishi T, Fujikawa R, Kastian RF, Sakumura Y, Inagaki N. Analyses of actin dynamics, clutch coupling and traction force for growth cone advance. *J Vis Exp*. 2021;176:e63227.
23. Higashiguchi Y, Katsuta K, Minegishi T, Yonemura S, Urasaki A, Inagaki N. Identification of a shootin1 isoform expressed in peripheral tissues. *Cell Tissue Res*. 2016;366:75–87.
24. Winzeler A, Wang JT. Purification and culture of retinal ganglion cells. *Cold Spring Harb Protoc*. 2013;2013:614–617.

25. Qiu Z, Minegishi T, Aoki D, Abe K, Baba K, Inagaki N. Adhesion-clutch between DCC and netrin-1 mediates netrin-1–induced axonal haptotaxis. *Front Mol Neurosci*. 2024;17:1307755.
26. Kastian RF, Minegishi T, Baba K, et al. Shootin1a-mediated actin-adhesion coupling generates force to trigger structural plasticity of dendritic spines. *Cell Rep*. 2021;35:109130.
27. Sapir T, Levy T, Sakakibara A, Rabinkov A, Miyata T, Reiner O. Shootin1 acts in concert with KIF20B to promote polarization of migrating neurons. *J Neurosci*. 2013;33:11932–11948.
28. Kubo Y, Baba K, Toriyama M, et al. Shootin1–cortactin interaction mediates signal–force transduction for axon outgrowth. *J Cell Biol*. 2015;210:663–676.
29. Sapir T, Levy T, Kozer N, et al. Notch activation by shootin1 opposing activities on 2 ubiquitin ligases. *Cereb Cortex*. 2017;3115–3128.

Investigative Ophthalmology & Visual Science